J Artif Organs (2012) 15:364–374
DOI 10.1007/s10047-012-0650-8

ORIGINAL ARTICLE

# Numerical comparison of the closing dynamics of a new trileaflet and a bileaflet mechanical aortic heart valve

**Chi-Pei Li · Po-Chien Lu**

Received: 13 January 2012 / Accepted: 8 May 2012 / Published online: 13 June 2012


**Abstract** The closing velocity of the leaflets of mechanical heart valves is excessively rapid and can cause the cavitation phenomenon. Cavitation bubbles collapse and produce high pressure which then damages red blood cells and platelets. The closure mechanism of the trileaflet valve uses the vortices in the aortic sinus to help close the leaflets, which differs from that of the monoleaflet or bileaflet mechanical heart valves which mainly depends on the reverse flow. We used the commercial software program Fluent to run numerical simulations of the St. Jude Medical bileaflet valve and a new trileaflet mechanical heart valve. The results of these numerical simulations were validated with flow field experiments. The closing velocity of the trileaflet valve was clearly slower than that of the St. Jude Medical bileaflet valve, which would effectively reduce the occurrence of cavitation. The findings of this study are expected to advance the development of the trileaflet valve.

**Keywords** Mechanical heart valve · Valve closing dynamics · Fluid–structure interaction

## Introduction

Mechanical heart valve (MHV) replacement surgery has become a prevalent and efficient treatment option for many cardiac patients. However, recipients require lifelong anticoagulant medications to reduce the risk of thrombosis and thromboembolism [1, 2]. Early research revealed that major factors in thrombosis and thromboembolism include cavitation phenomenon at the instant of valve impact [3–6] and the shear stresses in the flow fields or stagnant flow through the MHV [7–9]. The cavitation phenomenon is caused by a combination of the water hammer effect, squeeze flow, Venturi effect, and vortices in the flow fields, among which the Venturi effect and vortices have been shown to play minor roles [10, 11]. The water hammer effect is caused by the valve leaflets impacting the housing over a very short time, while the magnitude of the squeeze flow is relative to the velocity of valve closure. Therefore, the influence of these two factors can be minimized if the velocity of valve closure is slower. At the aortic valve position, the flow field and valve closure behavior are influenced by interactions between the vortices in the aortic sinus and the geometry of the MHV. Early studies on MHVs revealed that the mechanisms of closure differ among monoleaflet, bileaflet, and trileaflet valves [12], with those of the monoleaflet and bileaflet valves being dependent on reverse flow during their cardiac cycles and that of the trileaflet valve being mainly due to vortices in the aortic sinus. Consequently, the trileaflet valve closes more slowly (>50 ms) than the monoleaflet or bileaflet valves (<35 ms), which would effectively minimize the occurrence of cavitation.

Because the leaflets and the valve housing are opaque, taking velocity measurements with non-invasive laser velocimeters becomes impracticable. Laser Doppler velocimetry (LDV) only provides flow information at a single point in space and time. High-resolution dynamic particle image velocimeter (PIV) has been used to map the velocity vector fields and Reynolds stresses in the immediate downstream of aortic mechanical valves [13].

C.-P. Li (✉) · P.-C. Lu (✉)
Department of Water Resources and Environmental Engineering, Tamkang University, 151 Ying-Chuan Road, Tamsui, New Taipei 251, Taiwan
e-mail: 894330017@s94.tku.edu.tw

P.-C. Lu
e-mail: lupc@mail.tku.edu.tw

However, it is acknowledged that due to intrinsic limitations the PIV can only provide two-dimensional (2D) cross-sections of the flow fields. High-resolution 3D measurements are very challenging to obtain due to both time and cost. For these reasons, numerical simulations have been more commonly applied in recent years to study the flow fields across MHVs [14–25]. Although numerical simulations are convenient to acquire data of flow fields across MHVs, the pulsatile flow and complex geometric structures of MHVs remain difficult issues to simulate.

In this study, the turbulence $k$–$\omega$ model, which is suitable for a low Reynolds number and transitional flow, and the fluid–structure interaction (FSI) method by Nobili et al. [14] and Redaelli et al. [15] were applied to simulate the interactions between the leaflets and the fluid. The leaflet motion over the full cardiac cycle was computed, and the results were validated with experimental data [26]. A well-designed numerical simulation model of leaflet motions and flow fields is expected to assist and improve valve design in the future.

## Materials and methods

In this study, a 27-mm new type trileaflet (TRI) valve and a St. Jude Medical (SJM) 27-mm bileaflet valve (Fig. 1) were used as the test valves mounted in the aortic position. The new design of the trileaflet artificial heart valve opens such that the blood flows hemodynamically through a single central orifice flow, which closely resembles the action of physiologic valves. The fan-shaped leaflets are curved to form a circular central orifice and maximize the effective area. On the annulus ring, there are three small projections with smooth round sockets on both sides that serve as the leaflet hinges. The leaflets themselves also have notches on opposite sides, which give each leaflet round pivots that fit smoothly into the sockets. When the leaflets close, the projections on the valve ring serve to block blood flow through the notches on the leaflets. The notches and ball-in-socket hinges place the axes of rotation for the leaflets closer to the upstream side of the valve and increase the rotational inertia. The leaflets are freely suspended within the hinges, thus leading to lower mechanical resistance and more space for rotational motion when the leaflets open and close.

Figure 2 shows the schematic diagram of the computational domain. The diameter of the aorta was 25 mm. The aortic sinus had a diameter of 36 mm and was axis-symmetric in shape. The total length of the calculating domain was 130 mm. The angles were 25° and 85° between the $x$-axis and the leaflet when the SJM valve was fully closed and fully opened, respectively. Therefore, the traveling angle between fully closed and opened was 60°. Similarly, the angles were 45° and 90° between the $x$-axis and the leaflet when the TRI valve was fully closed and fully opened, respectively. Hence, the traveling angle was 45°. Because of geometric symmetry and in order to save costs and time, only half of the computational domain was simulated with the SJM valve, and the faces in the middle plane were set to symmetric conditions. Similarly, only one-third of the computational domain was simulated with the TRI valve, and the faces in the connected plane were set to symmetric conditions. In real flow, the leaflets exhibit unsynchronized closing behavior, which requires separate calculations for each leaflet and creates more complicated flow conditions. From an experimental standpoint, measuring the full domain under those circumstances would be a separate study in turbulence statistics. As the primary aim of our study was to improve the trileaflet MHV design through numerical calculations, we assumed synchronized closing behavior to focus on individual leaflets.

The geometry and mesh were created with the software program Gambit 2.2, and the meshes consisted of tetrahedral grids of 0.5 mm size. The numerical simulations were calculated with the software Fluent 6.3, which uses the

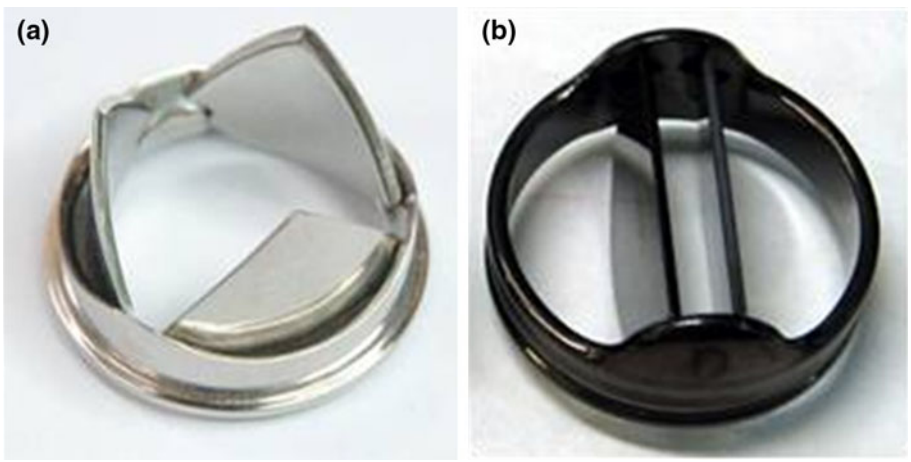


**Fig. 1** **a** Trileaflet (TRI) valve, **b** St. Jude Medical valve (SJM)

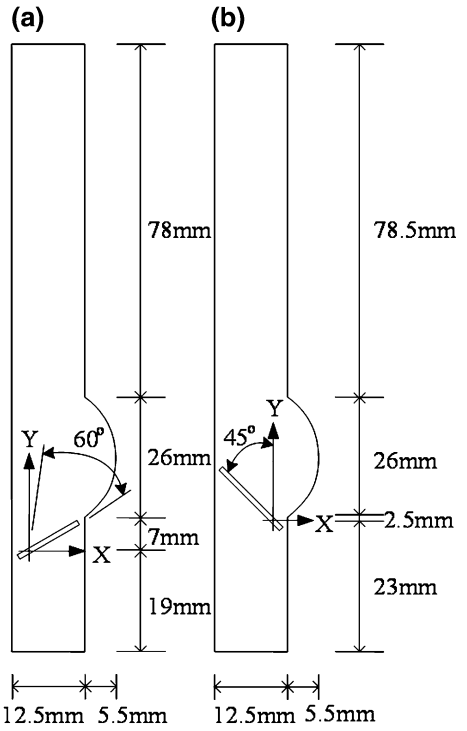


**Fig. 2** Schematic diagram of the computational domain. **a** SJM valve, **b** (TRI) valve. $D = 25$ mm

finite-volume method to solve the equations of fluid dynamics. The total numbers of cells applied in the simulations were 1,383,229 for the SJM valve and 542,333 for the TRI valve. The gaps between the leaflets and between each leaflet and the valve housing could not be zero because the process of calculations would appear as error messages. Thus, the geometries of the SJM leaflet were slightly modified, and we kept a gap of 0.25 mm between the leaflet and the middle plane of symmetric conditions. Similarly, a gap of 0.25 mm was also kept between the leaflet and the valve housing. For the TRI valve, the leaflet was scaled by a factor of 0.95 and moved 0.3 mm forward to the valve housing, and the valve housing was scaled by a factor of 1.05 in order to avoid any interference during the rotational motion of the leaflet.

Inlet boundary conditions were set to a velocity inlet, and outlet boundary conditions were set to a pressure outlet based on the experimental data of the flow rate and aortic pressures, as shown in Fig. 3. The velocity of the inlet was obtained by the flow rate divided by the cross-sectional area of the inlet. Due to complex flow fields of pulsatile flow across the MHV, the standard $k$–$\omega$ turbulence model that is suitable for low Reynolds number and transitional flow was applied in the simulations. In order to validate the experimental data, a heart rate of 70 bpm was used. The blood was modeled as an incompressible and Newtonian fluid with a density of $\rho = 1.287$ g/cm$^3$ and a dynamic viscosity of 3.9 cP.

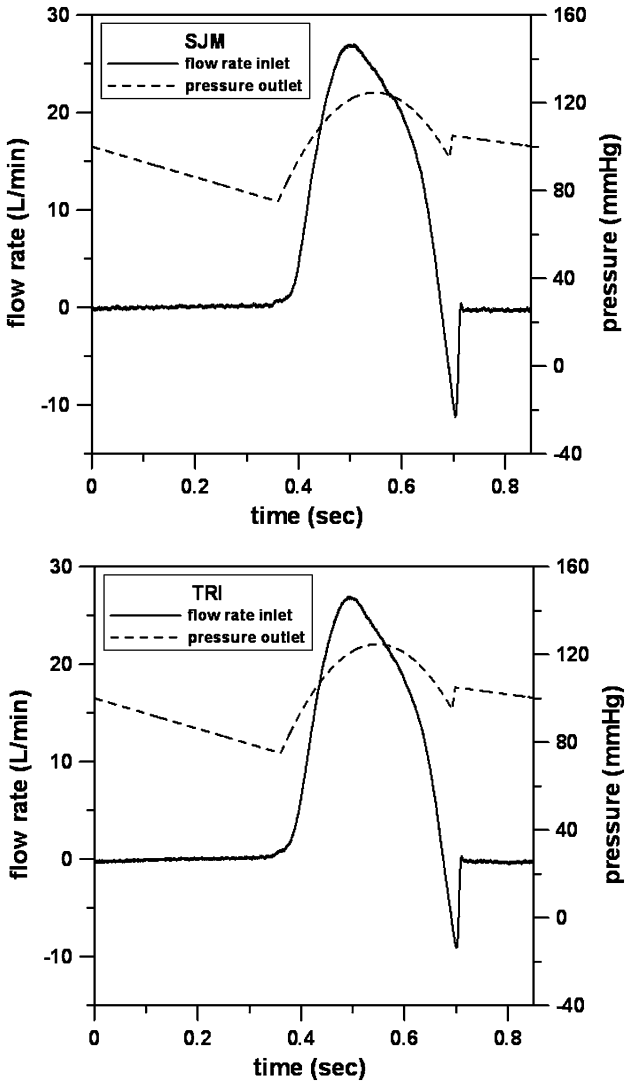


**Fig. 3** Inlet and outlet boundary conditions by the aortic flow rate and pressure over a cardiac cycle for the SJM valve (**a**) and TRI valve (**b**)

In this study, the motions of the valve leaflets were simplified to rigid body rotations along the $z$-axis. For the fluid–structure interactions, the methods of Nobili et al. [14] and Redaelli et al. [15] were applied in the simulations. At the end of the $n$th time step, the total moment $M_p$ acting on the leaflet due to the fluid pressures was calculated as

$$M_p = \sum_{i=1}^{n_b} (p_i A_i n_i) \times r_i \quad (1)$$

where $n_b$ was the number of the leaflet boundary faces, $p_i$ was the pressure on the face, with its vector indicated with $n_i$, $A_i$ was the area of the face, and $r_i$ was the distance from the rotation axis. The effects of shear stresses and gravity on the leaflet were not considered in Eq. (1).

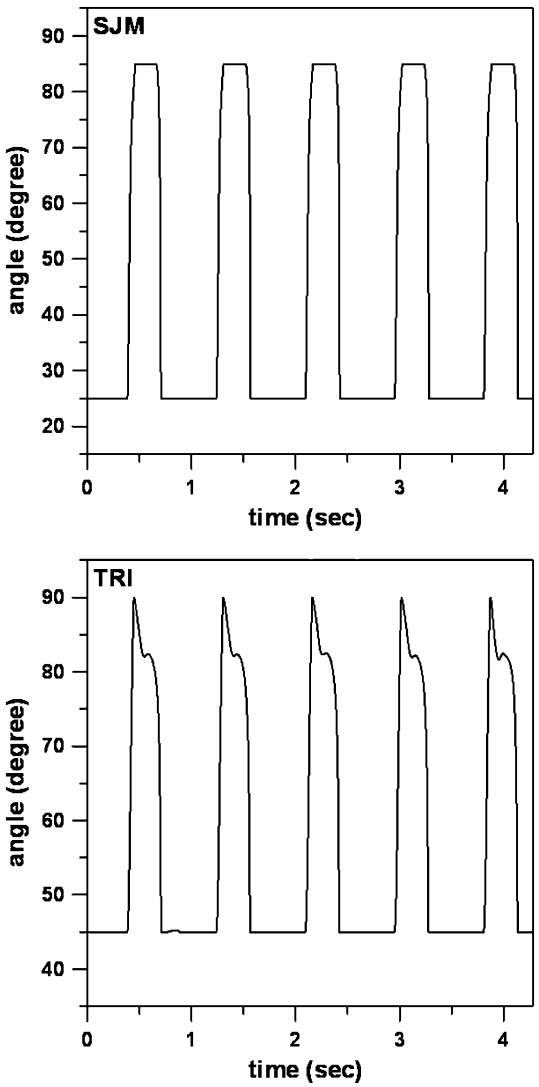


**Fig. 4** Leaflet motions over five cycles for the SJM valve (**a**) and TRI valve (**b**)

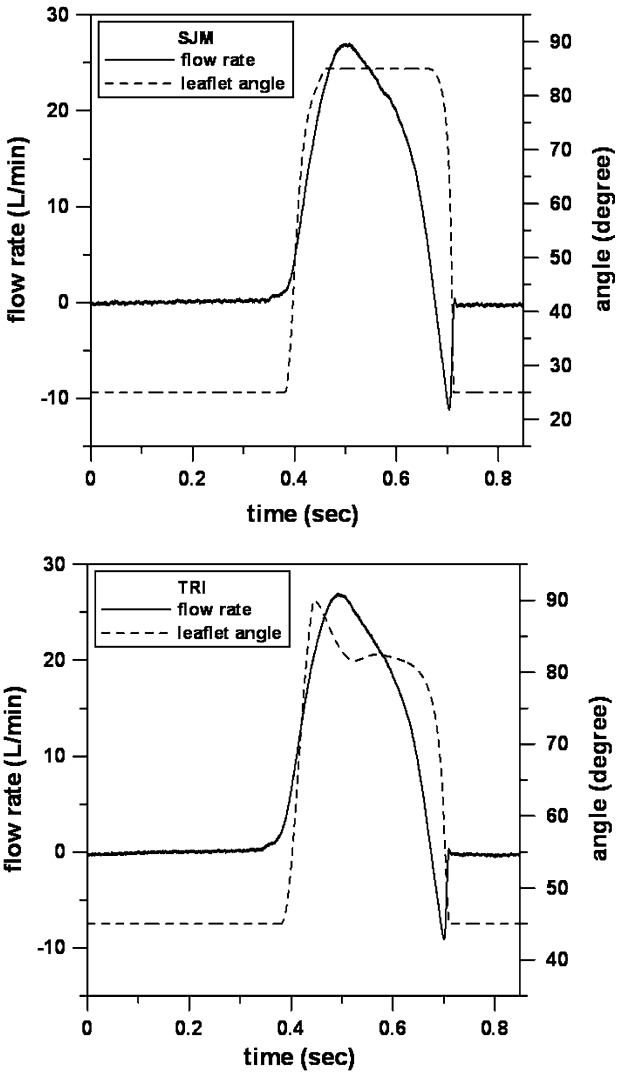


**Fig. 5** Aortic flow rate and leaflet motions during the fifth cardiac cycle for the SJM (**a**) valve and TRI valve (**b**)

After the value of $M_{\mathrm{p}}$ was calculated, the angular acceleration of the leaflet at the current $n$th time step could be calculated as

$$M_p = I\frac{\mathrm{d}^2\theta}{\mathrm{d}t^2} \tag{2}$$

where $I$ was the moment of inertia of the leaflet, $\theta$ was the rotation angle of the leaflet, $t$ was the time, and thus $\frac{\mathrm{d}^2\theta}{\mathrm{d}t^2}$ was the angular acceleration of the leaflet. Because the primary material of the SJM leaflet was pyrolytic carbon with a density of 2,230 kg/m$^3$, the moment of inertia of the SJM leaflet was $1.2 \times 10^{-8}$ kg m$^2$. The primary material of the TRI leaflet was titanium with a density of 4,507 kg/m$^3$, so the moment of inertia of the TRI leaflet was $9.167 \times 10^{-8}$ kg m$^2$.

After the value of $M_{\mathrm{p}}$ was calculated, the angular acceleration of the leaflet at the next time step, or $(n+1)th$ step, could be calculated as

$$\ddot{\theta}_{n+1} = \ddot{\theta}_{n} + w(M_{p,n}/I - \ddot{\theta}_{n}) \tag{3}$$

where $w$ was the under-relaxation factor, which could reduce the damping changes in the acceleration produced during each iteration. If the value of $w$ was set extremely high, the simulation would be unstable or exhibit divergence. In this study, $w$ was set to 0.05.

Finally, the Newmark method [27, 28] was applied to calculate the leaflet angle at the $(n+1)$-th time step as

$$\dot{\theta}_{n+1} = \dot{\theta}_{n} + \Delta t\,\ddot{\theta}_{n+1} \tag{4}$$

$$\theta_{n+1} = \theta_{n} + \Delta t\,\dot{\theta}_{n} + \Delta t^2\,\ddot{\theta}_{n+1} \tag{5}$$

where $\Delta t$ was the time step size in the simulations.

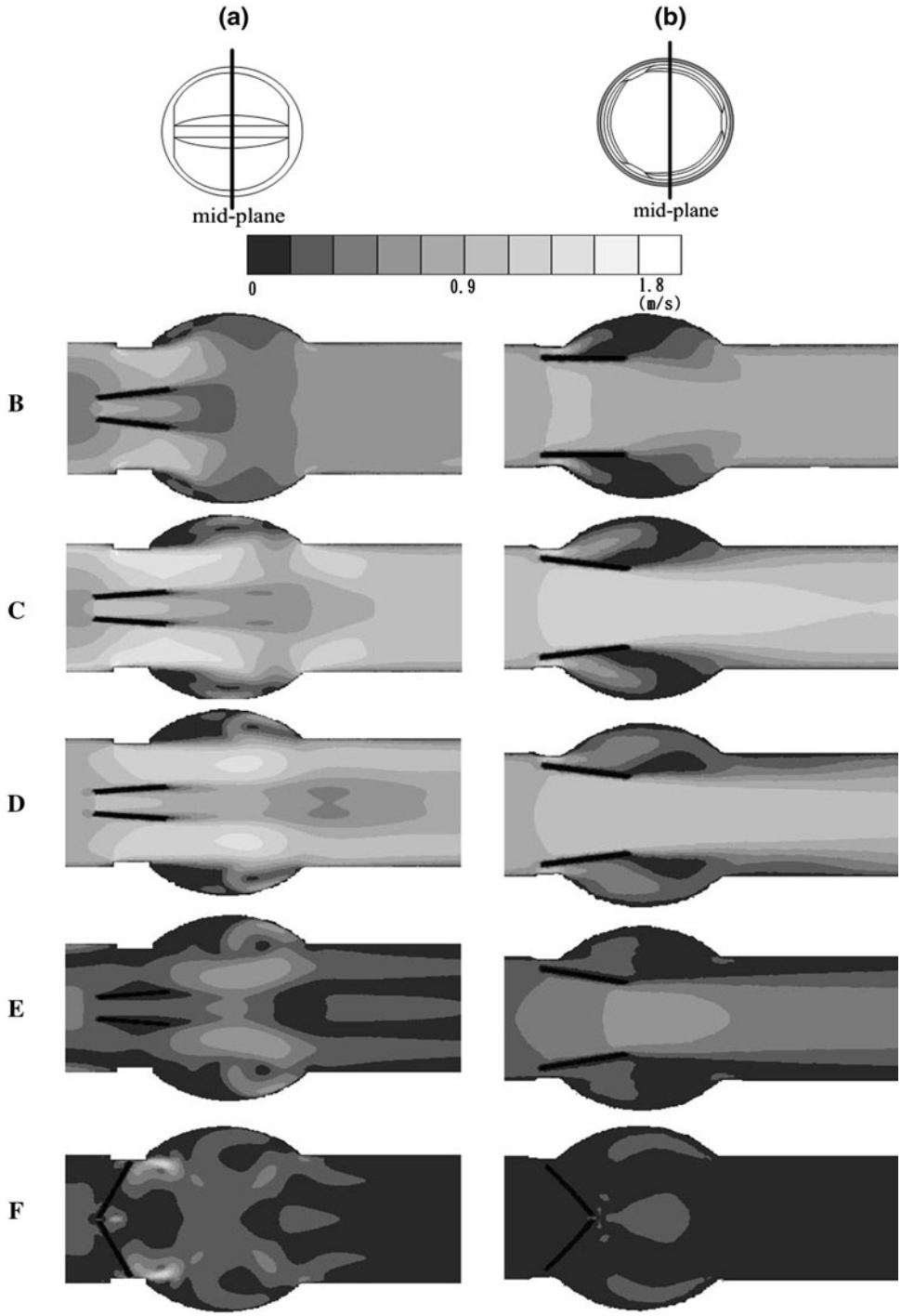


**Fig. 6** Contours of velocity magnitude in the middle plane during the fifth cardiac cycle for the SJM valve (**a**) and TRI valve (**b**) at different phases, namely, fully open (*B*), peak systole (*C*), 60 ms after peak systole (*D*), start of closure process (*E*), and fully closed (*F*)

In this study, the time step size ($\Delta t$) was set to 0.1 ms, and each time step iterated 20 times for the calculations. The simulations were run in parallel on 15 Intel 2.53 GHz CPU processors with 16 GB RAM. One cardiac cycle of the simulations took about 16 h for the SJM valve and 13 h for the TRI valve. In order to reduce the influence from the initial conditions, we analyzed only the flow fields of the fifth cardiac cycle after simulations of five cardiac cycles. The leaflet angles over five cardiac cycles are shown in Fig. 4.

## Results

The angles of the leaflets over time during the fifth cardiac cycle are shown in Fig. 5. For the SJM valve, the leaflet

**Table 1** Time history and the maximum velocity values of velocity for the St. Jude Medical valve during each phase

| Phase | Valve motion | Time of experiment (ms) [25] | Time of CFD (ms) | Maximum velocity in experiment (m/s) [25] | Maximum velocity in CFD (m/s) |
|---|---|---|---|---|---|
| A | Starting to open | 380 | 380 | NA | 0.13 |
| B | Fully open | 440 | 460 (437 at 80) | 1.06 | 1.51 (1.27) |
| C | Peak systole | 500 | 500 | 1.53 | 1.72 |
| D | 60 ms after peak systole | 560 | 560 | 1.33 | 1.47 |
| E | Starting to close | 670 | 672 | 0.49 | 0.66 |
| F | Fully closed | 700 | 712 | 0.37 | 5.17 (in gap) |

*CFD* Computational fluid dynamics, *NA* not available

started to open at 380 ms, and the leaflet angle was 80° at 437 ms. Even though the leaflet was fully opened at 460 ms and the duration of the fully opening process was about 80 ms, the final 5° of opening took more than 20 ms.

During the opening process of the SJM valve, the angular velocity of the leaflet increased to a maximum value of 1,765°/s (or 30.8 rad/s) at 399 ms and then decreased with time. When the opening angle of the leaflet was 80° and thus very close to the fully opened angle of 85°, the effective moment due to the axial flow on the leaflet decreased; consequently, the angular velocity also decreased to 291°/s and the rotation of the leaflet would be very slow. Therefore, there may be significant inaccuracies in estimating the time of the opening process. Based on this result, a reasonable estimate of the duration of SJM leaflet opening should be 57 ms.

During the closure process of the SJM valve, the leaflet started to close at 672 ms and was fully closed at 712 ms; consequently, the duration of the closing process was 40 ms. During valve closure, the angular velocity of the leaflet increased over time to the maximum value of 8,382°/s (or 146.3 rad/s) at the instant of full closure.

For the TRI valve, the leaflet started to open at 380 ms. During the opening process of the TRI valve, the angular velocity of the leaflet reached a maximum value of 1,037°/s (or 18.1 rad/s) at 414 ms and then decreased with time. After 414 ms, the effective moment from axial flow on the leaflet became smaller. At 444 ms, the leaflet was fully opened and the angular velocity was 426°/s; hence, the duration of the fully opening process was 64 ms. After the valve was fully opened at 90°, the leaflet closed slightly back to 82° where it reached a temporal balance.

The leaflet of the TRI valve started to close during the closing process at 650 ms. The angular velocity of the leaflet increased to a maximum value of 1,684°/s (or 29.4 rad/s) at 701 ms and then decreased with time. At 710 ms, the leaflet was fully closed, and the angular velocity was 1,054°/s (or 18.4 rad/s); consequently, the duration of the entire closing process was 60 ms.

The leaflet of the TRI valve would not maintain the fully opened position after valve opening, and there was an angle of 8° between the balanced position and the fully opened position. The leaflet angle of this balanced position indicated that the moment due to the jet flow across the minor orifice might push the leaflet backwards. As seen on the velocity fields, there is an obvious difference between the flow velocities on either side of the leaflet when the TRI valve is fully open, with the central orifice flow being faster than the minor orifice flow. Given the inverse relation between flow velocity and pressure, the moment produced by the minor orifice jet flow exerts enough pressure to push the leaflet back from the fully opened to the balanced position of 8°. In addition, when the flow rate decreased to less than 10 L/min, the leaflet started to close due to the decrease of the moment produced by the jet flow across the major orifice.

Figure 6a shows the contours of the velocity magnitude in the middle plane at selected phases (Table 1) through the fifth cardiac cycle for the SJM valve. At the peak flow phase of 500 ms, the two leaflets of the SJM valve divided the cross-sectional area into three orifices, and thus there were three jet flows. These jet flows gradually developed with time and connected downstream to become a continuous flow field. The maximum velocity was 1.72 m/s. After the leaflets closed, there were three jet flows across the gaps between two leaflets and the valve housing.

Figure 6b shows the contours of the velocity magnitude in the middle plane at selected phases during the fifth cardiac cycle for the TRI valve. At the peak flow phase of 500 ms, the leaflets divided the cross-sectional area into a major orifice and three minor orifices, and thus a central flow and three jet flows passed through the major orifice and each minor orifice, respectively. The central flow of the major orifice developed gradually and subsequently dissipated downstream of the valve with the decrease in flow rate. The maximum velocity was 1.55 m/s. After the leaflets closed, there was no apparent jet flow across the central gap between the leaflets.

Figure 7a demonstrates the contours of the vorticity magnitude in the middle plane at selected phases (Table 2) during the fifth cardiac cycle for the SJM valve. After the leaflets started to open, vortices gradually developed with

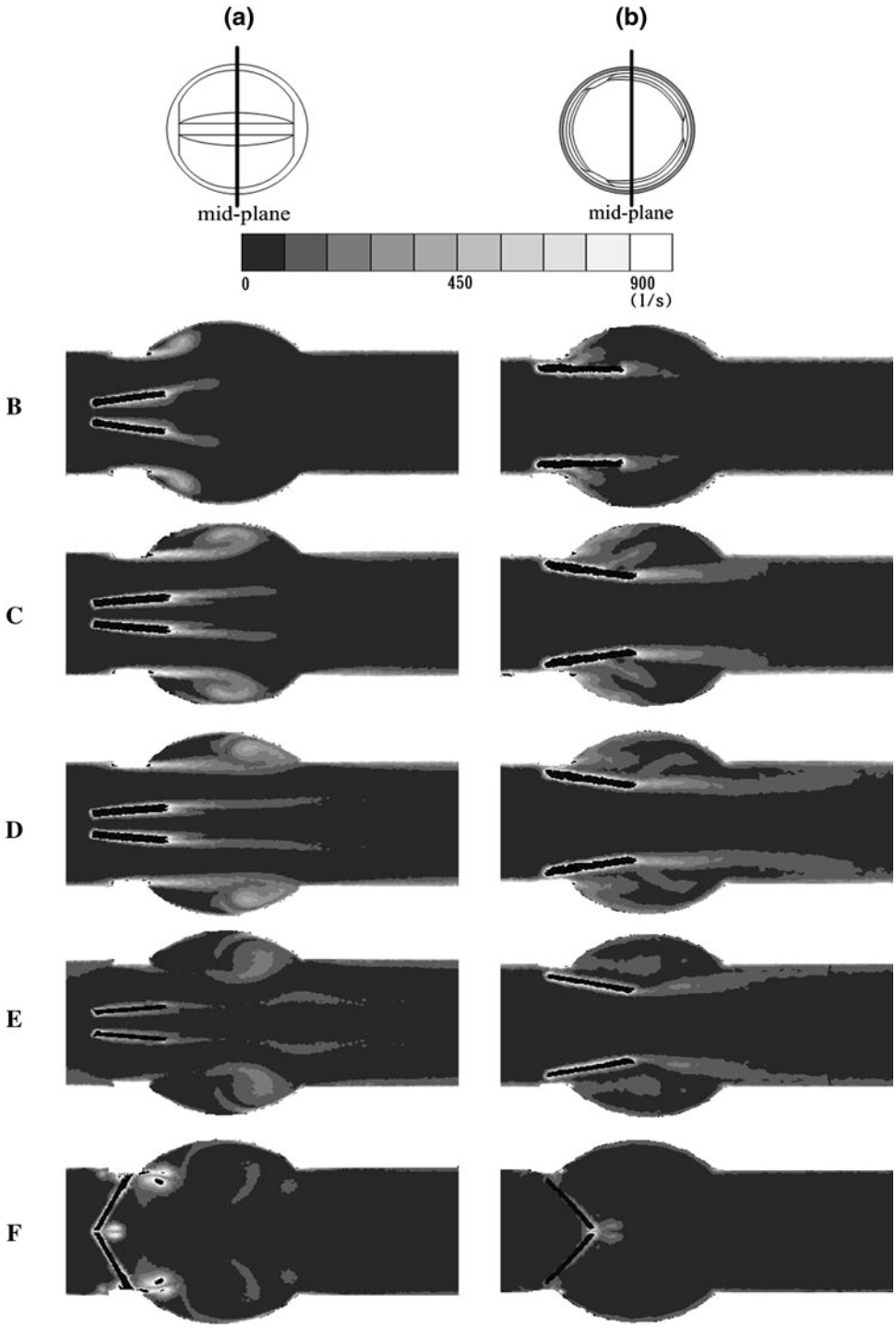


**Fig. 7** Contours of vorticity magnitude in the middle plane during the fifth cardiac cycle for the SJM valve (**a**) and TRI valve (**b**) at different phases, namely, fully open (*B*), peak systole (*C*), 60 ms after peak systole (*D*), start of closure process (*E*), and fully closed (*F*)

time in the wake flows downstream of the leaflets and within the aortic sinus; these vortices subsequently slowly moved downstream with the jet flows. Before the leaflets started to close at 660 ms, the vortices apparently distributed downstream of the aortic sinus. During the closing process of the leaflets, the vortices distributed near the orifices of the leaflets. After the leaflets fully closed, there were obvious vortices with three jet flows across the gaps between the two leaflets and the valve housing. The maximum vorticity magnitude was approximately 800 $s^{-1}$ during the opening process and 1400 $s^{-1}$ after the leaflets closed.

Figure 7b illustrates the contours of the vorticity magnitude in the middle plane at selected phases during the fifth cardiac cycle for the TRI valve. After the leaflets began to open, vortices gradually developed over time at the

**Table 2** Time history and the maximum velocity values for the trileaflet valve during each phase

| Phase | Valve motion | Time of experiment (ms) [25] | Time of CFD (ms) | Maximum velocity in experiment (m/s) [25] | Maximum velocity in CFD (m/s) |
|---|---|---|---|---|---|
| A | Starting to open | 380 | 380 | NA | 0.07 |
| B | Fully open | 450 | 444 | 1.56 | 1.08 |
| C | Peak systole | 500 | 500 | 2.09 | 1.55 |
| D | 60 ms after peak systole | 560 | 560 | 1.69 | 1.26 |
| E | Starting to close | 650 | 650 | 0.91 | 0.60 |
| F | Fully closed | 700 | 710 | 0.45 | 0.68 (in gap) |

wake flows downstream of the leaflets and in the aortic sinus. These vortices slowly combined together, and the whole aortic sinus subsequently was filled with vortices. When the leaflets started to close, these vortices re-distributed near the central flow across the major orifice. After the leaflets fully closed, there was no obvious vortex on both sides of the central flow across the central gap. The maximum vorticity magnitudes were approximately 1,100 $s^{-1}$ during opening and 1,200 $s^{-1}$ after the leaflets closed.

In order to compare the results from the numerical model and experimental data, six phases were selected, as shown in Table 1 for the SJM valve and Table 2 for the TRI valve. The maximum velocities during each phase were similar in magnitude with the results of the experiments. However, at the phase of full valve closure, the maximum velocity within the gap suddenly spiked due to the decrease of cross-sectional area.

## Discussion

For the SJM valve, the motions of opening and closing took 57 and 40 ms, respectively; in comparison, the motions of opening and closing for the TRI valve took 64 and 60 ms, respectively. This difference indicates that the opening and closing processes were more time-consuming for the TRI valve than the SJM valve, especially in terms of the duration of valve closure. Because the traveling angles were 60° for the SJM valve and 45° for the TRI valve, the closing velocity of the TRI valve was slower than that of the SJM valve.

The rotational radii were about 10 mm for the SJM valve and 13 mm for the TRI valve. At the instant of valve closure, the angular velocity of the SJM valve was 146.3 rad/s, while that of the TRI valve was merely 18.4 rad/s. Based on these data, the tip velocity of the leaflet of the SJM valve was approximately 1.46 m/s, while that of the TRI valve was only 0.24 m/s.

The different closing velocities of the leaflets between these two valves can be explained by the mechanisms of valve closure. When the SJM valve was fully opened, there was an angle of 5° between the valve leaflets and the flow. As the flow decreased, the reverse flow due to the pressure gradient between the aorta and the left ventricle pushed the leaflets to close. The mechanism of the TRI valve closure was quite different. Because the angle between the leaflets and the direction of the axial flow was almost zero when the TRI valve was fully opened, the reverse flow could not effectively contribute to push the leaflets to close. Thus, the leaflets were mainly pushed by the vortices in the aortic sinus, resulting in the TRI valve starting to close much earlier than the SJM valve.

Bellhouse and Talbot [29] studied the closure mechanism of the human aortic valve, and their results indicate that there is a vortex within each aortic sinus and that these vortices would benefit from the closure of the valve leaflets. Three-quarters of the valve's closure was accomplished during forward flow, with very little reverse flow required to seal it. The same kind of closure mechanism occurred with the TRI valve in this study (Fig. 8).

The leaflets' closing behavior was considered to be an important factor in MHV cavitation [30]. Lee et al. [31] used six different kinds of monoleaflet and bileaflet valves that were mounted in the mitral position in an electrohydraulic total artificial heart. Their results show that the closing velocity of the bileaflet valves is slower than that of the monoleaflet valves. These researchers found that cavitation bubbles were concentrated on the edge of the valve stop and along the leaflet tip, and thus it was established that squeeze flow holds the key to MHV cavitation. Cavitation intensity also increases with an increase in the valve closing velocity and the valve stop area.

Li et al. [26] measured the opening and closing time with the axis-symmetric aortic sinus. Two leaflets of the SJM valve took 60.5 ± 2.6 and 59.8 ± 2.4 ms, respectively, during the opening phase, and the results of the simulation in this study was 57 ms. During the closing phase, two leaflets of the SJM valve took 30.1 ± 2.2 and 29.7 ± 3.1 ms to close, and the results of this simulation was 40 ms. These results indicate that the results of the cost-time by numerical simulations were slightly overestimated and that the real angular velocities of the SJM valve

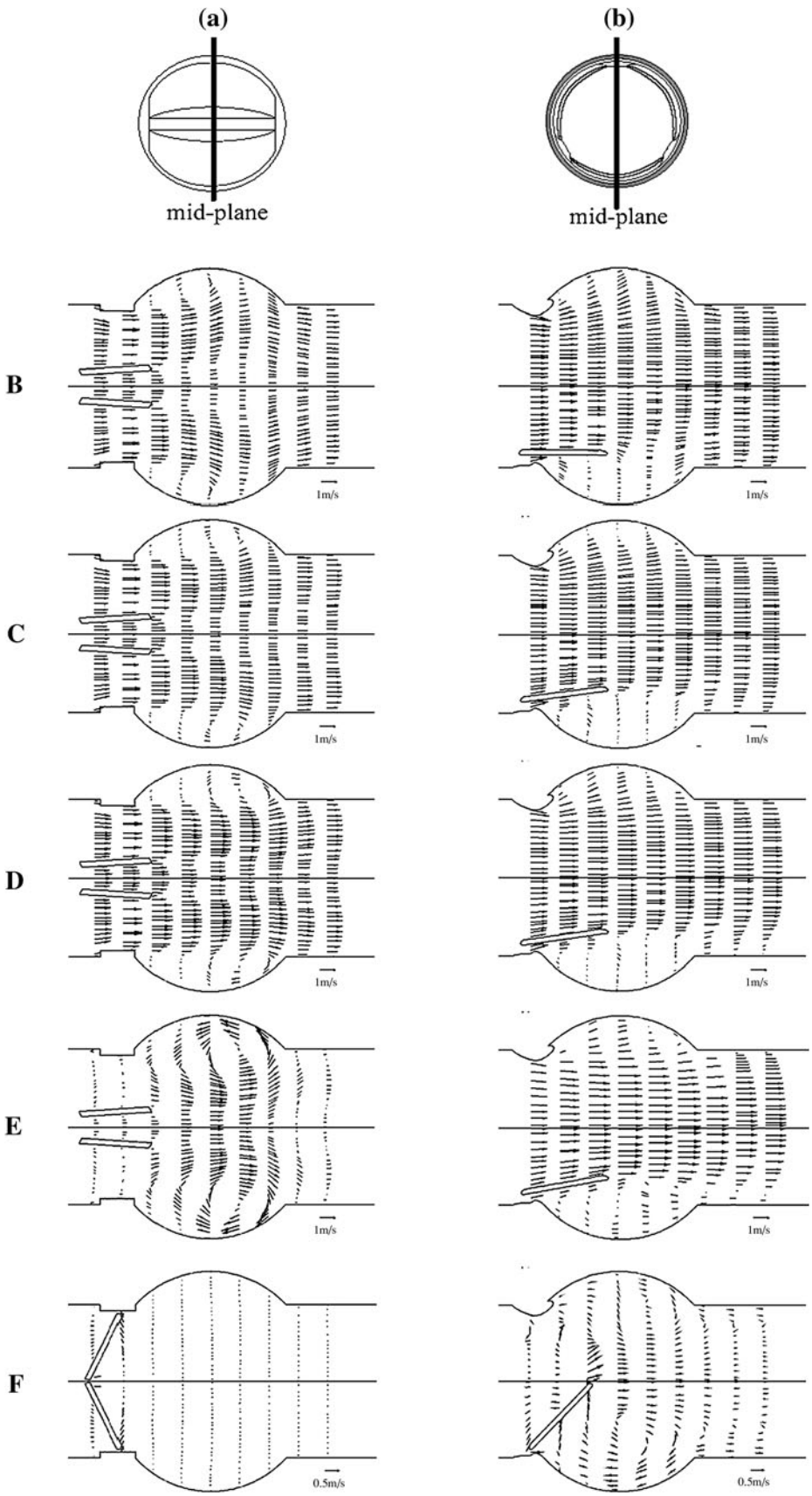


**Fig. 8** Velocity profiles in the plane of the middle of the leaflet during the fifth cardiac cycle for the SJM valve (**a**) and TRI valve (**b**) at different phases, namely, fully open (*B*), peak systole (*C*), 60 ms after peak systole (*D*), start of closure process (*E*), and fully closed (*F*)

should be larger than the simulations. As already mentioned, because of error messages during the calculation process, we slightly modified the geometries of the SJM leaflet, maintaining a gap of 0.25 mm between the leaflet and the middle plane of symmetry conditions. The size of this gap was much larger than the actual gap size, which was approximately 1.118 μm [14], and undoubtedly there would be limitations to creating meshes of 1 μm in size to run the simulation. In addition, the effects of shear stresses and gravity on the leaflet were not considered in Eq. (1). Based on these limitations in our study, the moments on the leaflets might be underestimated and the leaflets might rotate slower than the experimental results.

According to Li et al. [26], three leaflets of the TRI valve took 55.7 ± 6.8, 59.9 ± 7.4, and 62.4 ± 7.8 ms during the opening phase, and the results of the simulation in this study was 64 ms. During the closing phase, three leaflets of the TRI valve took 43.1 ± 3.7, 42.6 ± 2.5, and 43.3 ± 4.2 ms to close, and the results of the simulation was 60 ms. Similarly, the results of the cost-time by the numerical simulations were a little overestimated, and the real angular velocities should be larger than the simulations.

Nobili et al. [14] modeled the aortic sinus as three semi-spheres. Their experimental results showed that the closing time of the SJM valve was 33.24 ± 5.8 ms and their numerical result was 34 ms. These results are very similar to ours.

Lu et al. [12] simulated the aortic sinus as three semi-spheres, which obviously presents a different geometry than our axis-symmetric simulation. Their experimental results indicated that the opening and closing time of the SJM valve was 48 ± 2 and 30 ± 5 ms, respectively. These results were similar to the simulations in our study, which can be explained by the fact that the SJM valve relies on reverse flow to close and is not appreciably affected by the sinus geometry. Regarding the TRI valve in the previous study, the opening time was 50 ± 8 ms but the closing time was 80 ± 7 ms, which was much longer than the simulation in our study. The closure behavior of the TRI valve is affected by the recirculating vortex that forms within the aortic sinus; thus, the different geometries between three semi-spheres and an axis-symmetric sinus may be contributing to these differences in closing time. In addition, we speculate that the orientation of both SJM and TRI valves within a sinus formed by three semi-spheres, and therefore the orientation of individual leaflets, can affect the closing behavior. We applied an axis-symmetric sinus to avoid the influences of this geometry, but we also recognize that the interactions between the geometry and valve orientation will require further investigation.

Li et al. [26] measured the flow fields across the SJM valve by digital particle image velocimetry with an in vitro pulsatile mock circulatory loop system with axis-symmetric aortic sinus. Their results indicated the maximum velocity was approximately 1.53 m/s at peak flow phase; this value is similar to the simulation in this study. For the TRI valve, the maximum velocity was approximately 2.09 m/s, but the position of the maximum velocity was far away downstream of the valve, and the larger velocity might be produced by the narrowed aortic sinus. For the flow fields in the aortic sinus, the maximum velocity was approximately 1.6 m/s, and this value is very close to the results of our simulations.

Because of the different kinds of materials of these two valves, the moment of inertia of the TRI leaflet was much larger than that of the SJM leaflet. In addition, because the gap size of 0.25 mm was applied in this simulation for the SJM valve, which was much larger than the real gap size of approximately 1.118 μm, it should be possible to improve still further the flow fields in the gaps and the hinge.

According to the results of previous simulations, the time-step size also affects the accuracy of the simulations. Although the trajectories of the leaflet motions were similar, the timing would be closer to the experimental results if the time-step size was set to a smaller value. However, the cost-time for the simulations was also proportional to the time-step size. Based on these factors, we set the time-step size in the range of 0.01–0.05 ms.

In addition, the lack of experimental data accounting for different geometries of aortic sinuses, especially for the TRI valve and flow fields upstream of the valves, make it difficult to validate the results of these numerical simulations.

## Conclusions

In terms of leaflet opening and closing times and the times corresponding to the flow rate, the results of the simulations in this study are very similar to those reported previously. At peak flow phase, the distributions of velocity and vorticity also matched the values of the experiments, indicating that the results of the simulations were accurate in substance. Since the turbulence model was applied to solve turbulence flow and the boundary conditions were also simplified to ideal conditions, the variance in this study should be negligible.

Both the opening and closing times were longer for the TRI valve than for the SJM valve, and this phenomenon matched the results of prior experiments. The leaflets of the TRI valve would start to close earlier due to the vortices in the aortic sinus, and this closure mechanism certainly followed the concept of the design for the TRI valve. The slower leaflet motions during valve closure might effectively reduce occurrences of cavitation and risk of damage to red blood cells.

## References


1. Levine MN, Raskob G, Hirsh J. Hemorrhagic complications of long-term anticoagulation therapy. Chest. 1989;95:265–365.
2. Edmunds LHJ. Thrombotic and bleeding complications of prosthetic heart valves. Ann Thorac Surg. 1987;44:430–45.
3. Carey RF, Porter JM, Richard G, Luck C, Shu MCS, Guo X. An interlaboratory comparison of the FDA protocol for the evaluation of cavitation potential of mechanical heart valves. J Heart Valve Dis. 1995;4:532–41.
4. Hwang NHC. Cavitation potential of pyrolytic carbon heart valve prostheses: a review and current status. J Heart Valve Dis. 1998;7:140–50.
5. Kafesjian R, Howanec M, Ward GD, Diep L, Wagstaff LS, Rhee R. Cavitation damage of pyrolytic carbon in mechanical heart valves. J Heart Valve Dis. 1994;3:S2–7.
6. He Z, Xi B, Zhu K, Hwang NHC. Mechanicals of mechanical heart valve cavitation: investigation using a tilting disk valve model. J Heart Valve Dis. 2001;10:666–74.
7. Yoganathan AP, Corcoran WH, Harrison EC, Carl JR. The Bjork-Shiley aortic valve-prosthesis: flow characteristics, thrombus formation and tissue overgrowth. Circulation. 1978;58:70–6.
8. Liu JS, Lu PC, Chu SH. Turbulence characteristics downstream of bileaflet aortic valve prostheses. J Biomech Eng. 2000;122: 118–24.
9. Woo YR, Yoganathan AJ. In vitro pulsatile flow velocity and shear stress measurements in the vicinity of mechanical aortic heart valve prostheses. Life Support Syst. 1985;3:283–312.
10. Li CP, Lu PC, Liu JS, Lo CW, Hwang NHC. Role of vortices in cavitation formation in the flow across a mechanical heart valve. J Heart Valve Dis. 2008;17:435–45.
11. Gross JM, Guo GX, Hwang NHC. Venturi pressure cannot cause cavitation in mechanical heart valve prostheses. ASAIO J. 1991;37:M357–8.
12. Lu PC, Liu JS, Huang RH, Lo CW, Lai HC, Hwang NHC. The closing behavior of mechanical aortic heart valve prostheses. ASAIO J. 2004;50:294–300.
13. Akutsu T, Saito J, Imai R, Suzuki T, Cao XD. Dynamic particle image velocimetry study of the aortic flow field of contemporary mechanical bileaflet prostheses. J Artif Organs. 2008;11:75–90.
14. Nobili M, Morbiducci U, Ponzini R, Del Gaudio C, Balducci A, Grigioni M, Maria Montevecchi F, Redaelli A. Numerical simulation of the dynamics of a bileaflet prosthetic heart valve using a fluid-structure interaction approach. J Biomech. 2008;41: 2539–50.
15. Redaelli A, Bothorel H, Votta E, Soncini M, Morbiducci U, Del Gaudio C, Balducci A, Grigioni M. 3-D simulation of St. Jude Medical bileaflet valve opening process: fluid-structure interaction study and experiment validation. J Heart Valve Dis. 2004;13:804–13.
16. Dasi LP, Ge L, Simon HA, Sotiropoulos F, Yoganathan AP. Vorticity dynamics of a bileaflet mechanical heart valve in an axisymmetric aorta. Phys Fluids. 2007;19:067105.
17. Bluestein D, Rambod E, Gharib M. Vortex shedding as a mechanism for free emboli formation in mechanical heart valves. J Biomech Eng. 2000;122:125–34.
18. Alemu Y, Bluestein D. Flow-induced platelet activation and damage accumulation in a mechanical heart valve: numerical studies. Artif Organs. 2007;31:677–88.
19. Dumont K, Vierendeels J, Kaminsky R, Van Nooten G, Verdonck P, Bluestein D. Comparison of the hemodynamic and thrombogenic performance of two bileaflet mechanical heart valves using a CFD/FSI model. J Biomech Eng. 2007;129:558–65.
20. Dumont K, Stijnen JMA, Vierendeels J, Van De Vosse FN, Verdonck PR. Validation of a fluid-structure interaction model of a heart valve using the dynamic mesh method in Fluent. Comp Methods Biomech Biomed Eng. 2004;7:139–46.
21. Bang JS, Yoo SM, Kim CN. Characteristics of pulsatile blood flow through the curved bileaflet mechanical heart valve installed in two different types of blood vessels: velocity and pressure of blood flow. ASAIO J. 2006;52:234–42.
22. Choi CR, Kim CN. Numerical analysis on the hemodynamics and leaflet dynamics in a bileaflet mechanical heart valve using a fluid-structure interaction method. ASAIO J. 2009;55:428–37.
23. Ge L, Sotiropoulos F. A numerical method for solving the 3D unsteady incompressible Navier–Stokes equations in curvilinear domains with complex immersed boundaries. J Comput Phys. 2007;225:1782–809.
24. Sotiropoulos F, Borazjani I. A review of state-of-the-art numerical methods for simulating flow through mechanical heart valves. Med Biol Eng Comput. 2009;47:245–56.
25. Tullio MDD, Cristallo A, Balaras E, Verzicco R. Direct numerical simulation of the pulsatile flow through an aortic bileaflet mechanical heart valve. J Fluid Mech. 2009;622:259–90.
26. Li CP, Chen SF, Lo CW, Lu PC. Turbulence characteristics downstream of a new trileaflet mechanical heart valve. ASAIO J. 2011;57:188–96.
27. Dumont K, Vierendeels J, Verdonck PR. Feasibility study of the dynamic mesh model in Fluent for fluid-structure interaction of a heart valve. In: Brebbia CA, Arnez ZM, Solina F, Stankovski V, editors. Simulations in biomedicine V advances in computational bioengineering. Boston: WIT Press; 2003. p. 169–76.
28. Vierendeels J, Dumont K, Dick E, Verdonck PR. Stabilization of a fluid-structure coupling procedure for rigid body motion. In: Proc 33rd AIAA Fluid Dynamics Conference and Exhibit; 2003. p. 3720.
29. Bellhouse BJ, Talbot L. The fluid mechanics of the aortic valve. J Fluid Mech. 1969;35:721–35.
30. Lo CW. Causes of cavitation phenomena in mechanical heart valves. PhD. thesis. Tamkang University, Taipei, Taiwan; 2008.
31. Lee H, Taenaka Y, Kitamura S. Mechanisms of mechanical heart valve cavitation in an electrohydraulic total artificial heart. ASAIO J. 2005;51:208–13.